International Journal of Heat and Mass Transfer 52 (2009) 4796–4806

Contents lists available at ScienceDirect

International Journal of Heat and Mass Transfer

journal homepage: www.elsevier.com/locate/ijhmt

Mathematical modeling of the primary and secondary vacuum freeze drying of random solids at microwave heating

J.F. Nastaj *, K. Witkiewicz

Department of Chemical Engineering and Environmental Protection Processes, West Pomeranian University of Technology, Szczecin, 71-065 Szczecin, Al. Piastów 42, Poland

ARTICLE INFO

Article history:
Received 26 February 2009
Accepted 16 June 2009
Available online 16 July 2009

Keywords:
Freeze-drying
Primary stage
Secondary stage
Volumetric heating
Random solids

ABSTRACT

This paper presents a complex model of the primary and secondary vacuum freeze-drying stages at microwave heating. The simulation of the process was performed for typical adsorbents which were chosen as ideal representatives of random solids having particle and bed porosity. One-dimensional two-region model of the primary freeze-drying at microwave heating was formulated and then solved numerically using the finite-difference MacCormack method. Varying during the process sublimation front temperature $T_s(t)$ was taken into account. Simulated drying curves were compared with experimental results giving fairly good agreement. A mathematical model of the secondary freeze-drying at microwave heating was developed and solved using the numerical method of lines. Pressure drop in the material was taken into account and calculated using Ergun equation. As a result of the model solution, the moisture content and the temperature distributions in drying material were obtained. In both mathematical models steady internal heat source capacity was calculated as a function of material temperature.

1. Introduction

Freeze-drying is a multiple operation usually performed in three stages: pre-freezing of the wet product, primary drying when direct sublimation of the frozen solvent takes place in vacuum conditions, and finally secondary stage when residual bound water is desorbed from the material matrix [1–8]. Especially Liapis and Sadikoglu [7] and Sadikoglu et al. [8] derived comprehensive mathematical model of freeze-drying of pharmaceuticals at contact heating. In literature there are many papers concerning vacuum freeze-drying process at microwave heating [9–17]. Various general problems of microwave heating in physical systems are also developed [18–48]. In this paper, the complex mathematical model of both the primary and secondary freeze-drying at microwave heating is formulated.

The typical freeze-dried foodstuffs, pharmaceutical and biologic products have a porous, nonshrunken structure resulted from structural rigidity achieved by frozen water. However, some materials called random solids (disordered porous media) have a nonhomogenous inner structure which prevents collapse of the solid matrix [48]. The granular form of such materials means that both particle and bad porosity should be taken into consideration. Adsorbents being typical random solids were used here in theoretical and experimental investigation of the process.

2. Investigation of the primary freeze-drying of random solids at microwave heating

2.1. Experimental equipment

Experimental investigations of the primary freeze-drying of random solids at microwave heating were performed by means of the set-up composed of the microwave circuit, the vacuum system, the refrigeration system, the temperature and weight measurements devices and the data acquisition system (Fig. 1).

A cylindrical Teflon container filled with material to be dried is hanged on the extensometer balance inside the vacuum chamber. Temperature of dried material is measured by the fluoroptic thermometer (FOT Lab Kit – Luxtron Corp.) which does not interact significantly with electromagnetic field. The sample is inserted into the microwave applicator which is constructed as a section of rectangular brazen waveguide and acts as a mono-modal resonant cavity. One of applicator walls is the movable tuner and its position can be adjusted remotely by stepping motor. The applicator is considered to be tuned when current signal of the microwave detector coupled with the magnetic loop under the sample achieves maximum, which means maximal electric field strength in the sample.

Generated microwaves of 2450 MHz frequency are transmitted via the waveguide, the coaxial cable, the directional coupler and the vacuum feedthrough to the applicator inside the vacuum chamber. Microwave power reflected in the applicator returns to the directional coupler which directs it to the dummy load where is totally dissipated.

* Corresponding author. Tel.: +48 91 449 4084; fax: +48 91 449 4642.
E-mail address: jonas@ps.pl (J.F. Nastaj).

0017-9310/$ - see front matter © 2009 Elsevier Ltd. All rights reserved.
doi:10.1016/j.ijheatmasstransfer.2009.06.015

Nomenclature

a_e	effective thermal diffusivity, m^2/s
c_a	specific heat of adsorbed phase (water), J/(kg K)
c_{p_e}	effective specific heat, J/(kgK)
c_{p_g}	specific heat of gas phase, J/(kgK)
c_{p_g}	specific heat of gas phase in secondary freeze-drying, J/(molK)
c_{p_w}	specific heat of water vapor, J/(kgK)
c_s	specific heat of adsorbent, J/(kgK)
C	vapor molar concentration in secondary freeze-drying, mol/m^3
C_s	vapor mass concentration at sublimation front, equilibrium for T_s, kg/m^3
C_L	vapor mass concentration at material free surface, kg/m^3
C_∞	vapor mass concentration in vacuum chamber, kg/m^3
$D_{e_{II}}$	vapor diffusivity in dry layer, m^2/s
D_{eff}	effective diffusion coefficient, m^2/s
D_K	Knudsen diffusivity, m^2/s
D_M	molecular diffusivity, m^2/s
D_S	surface diffusion coefficient, m^2/s
D_{S0}	parameter in equation defining surface diffusion coefficient, m^2/s
d_z	particle diameter, m
E	electric field strength, V/m
E_0	activation energy, J/mol
f	microwave frequency, Hz
k_e	effective thermal conductivity, W/(m K)
K	kinetic coefficient, 1/s
K_{dys}	dissipation coefficient, $W/(mV^2)$
L	material layer thickness, m
M_{in}	molar mass of inert, kg/mol
M_w	molar mass of water, kg/mol
N_w	mass flux density diffusing from moving boundary, $kg/(m^2s)$
N_X	mass flux density diffusing from material in secondary freeze-drying, $mol/(m^2s)$
p_L	vapor partial pressure at material free surface, Pa
p_s	vapor partial pressure at sublimation front, equilibrium for T_s, Pa
P	vacuum chamber total pressure, Pa
q	heat flux, W/m^2
q_s	heat flux at moving boundary, W/m^2
Q_v	capacity of internal volumetric heat source, W/m^3
r_p	mean pore radius, m
R	universal gas constant, J/(molK)
t	time, s
t_p	initial time, s
T	temperature, K
$T_{II_{ref}}$	arbitrary reference temperature, K
$T_{II_{avg}}$	average temperature of region *II*, K
T_0	temperature of bottom surface, K
T_{con}	temperature of a condenser, K
T_L	exposed surface temperature, K
T_s	temperature of sublimation front at moving boundary, K
$T_{s,3}$	triple point temperature, K
$T_{s_{eq}}$	reference temperature (equilibrium temperature of ice sublimation), K
T_∞	surroundings temperature of the sample, K
W	average moisture content of dried bed, kg/kg
W_0	constant of the multitemperature Langmuir isotherm, kg/kg
W_{eq}	equilibrium moisture content, kg/kg
W_p	initial moisture content, kg/kg
W_r	equilibrium moisture content in secondary freeze-drying, kg/kg
x	Cartesian position coordinate, m
X	position coordinate of moving boundary, m
X_p	initial position coordinate of moving boundary, m
y_{in}	mole fraction of inert, mol/mol
y_w	mole fraction of water vapor, mol/mol
y_w^*	equilibrium mole fraction of water vapor, mol/mol

Greek symbols

α_{II_∞}	heat transfer coefficient at the surface of region *II*, $W/(m^2K)$
β_{II}	internal mass transfer coefficient in region *II*, m/s
ΔH_{ads}	heat of adsorption, J/mol
Δh_s	enthalpy of sublimation, J/kg
ε	porosity (–)
ε_0	permittivity of free space, F/m
ε''	relative loss factor (–)
$\varepsilon''_I, \varepsilon''_{II}$	effective relative loss factor in region *I* and region *II* (–)
ε_p	particle porosity (–)
η	gas viscosity, Pa s
μ_1	constant in Eq. (46) (secondary drying), $W/(mV^2\ K)$
μ_2	constant in Eq. (46) (secondary drying), $W/(mV^2)$
$\mu_{1_I}, \mu_{1_{II}}$	constants in Eqs. (4) and (7), respectively (primary drying), $W/(mV^2\ K)$
$\mu_{2_I}, \mu_{2_{II}}$	constants in Eqs. (4) and (7), respectively (primary drying), $W/(mV^2)$
ρ_{e_I}	effective density of region *I*, kg/m^3
ρ_{bu}	bulk density of dry material, kg/m^3
$\rho_{bu_{II}}$	bulk density of region *II*, kg/m^3
ρ_p	particle density of adsorbent, kg/m^3
σ_{AB}	characteristic length of the intermolecular force law [Lennard–Jones] (Å)
Ω_{AB}	collision integral for diffusion (–)

Dimensionless numbers

C_w^*	concentration of water in secondary freeze-drying
N_w^*	water vapor flux in region *II*
q_I^*, q_{II}^*	heat fluxes
Q_v^*	capacity of internal heat source in secondary drying stage
$Q_{v_I}^*, Q_{v_{II}}^*$	capacity of internal heat sources in primary freeze-drying stage
$Ste_{V_I}, Ste_{V_{II}}$	modified Stefan numbers
t^*, t_I^*, t_{II}^*	times
T_I^*, T_{II}^*	temperatures
W^*	average moisture content
x^*, x_I^*, x_{II}^*	dimensionless coordinates
X^*	moving boundary position
ω	pressure in secondary freeze-drying stage

Subscripts

I	frozen layer
II	dried layer
VC	vacuum chamber

Temperature inside the chamber is controlled by the refrigeration system with a refrigerant circulating in the vacuum chamber's jacket. Sublimated vapors are removed from the chamber by the cold trap cooled by means of liquid nitrogen. The vacuum pump is operating constantly whilst self-regulated purge valve maintains pressure in the vacuum chamber at the level of 100 Pa.

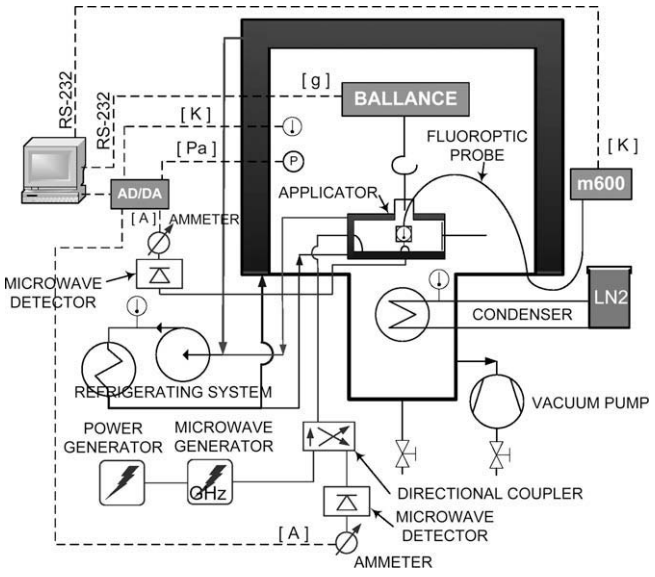

Fig. 1. The experimental set-up for investigations of the primary microwave freeze-drying.

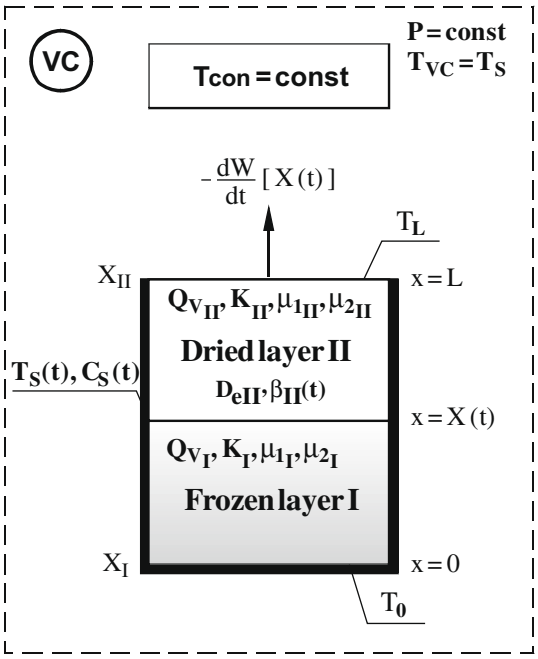

Fig. 2. A physical model of the primary freeze-drying of random solids at microwave heating.

2.2. Experimental methodology

Experiments of the primary microwave freeze-drying were performed two times: first with measurements of sample mass decrement and second with only sample temperature measurements. It was impossible to measure simultaneously both above mentioned values in the same experimental run. When temperature was measured, a fluoroptic probe was placed in the center of the sample.

After wet material freezing in the vacuum chamber at the temperature about −30 °C, the apparatus is sealed and the vacuum pump started. When demanded process pressure in the chamber is achieved, the microwave generator is turned on and the resonant cavity is tuned to a TE_{102} mode. During the single experimental run the sample temperature or sample weight decrement as well as temperature and pressure in the vacuum chamber are recorded by DASYLab data acquisition program. Additionally continuous measurements of current signal of the microwave detector coupled with magnetic loop inside the applicator indicates when the resonant cavity needs to be tuned during the experiments.

3. Mathematical model of primary freeze-drying of random solids at microwave heating

We consider a dried material having geometry of an infinite slab with bottom insulated and upper surface exposed to a vacuum at drying chamber temperature T_{VC}, as shown in Fig. 2.

The following assumptions are made to simplify governing equations:

(i) The sublimation ice front divides a sample into frozen region *I* and dried region *II* and its initial position X_p at $t = 0$ is arbitrary defined.
(ii) In frozen region *I* energy is transferred by conduction whereas conduction and convection are considered in dried region *II*.
(iii) During the process, as sublimated vapors diffuses from the interface towards exposed surface, moving boundary (ice front) retreats uniformly until frozen free water is totally removed.
(vi) In both material layers heat is generated as a result of microwaves absorption and dissipation.
(v) Distribution of electric field inside the microwave applicator is uniform.

3.1. Governing equations

3.1.1. Icy region

3.1.1.1. Energy conservation. In frozen region heat flux towards sublimation front is governed by:

$$\frac{\partial T_I}{\partial t} = a_{e_I}\frac{\partial^2 T_I}{\partial x^2} + \frac{Q_{v_I}}{\rho_{e_I} c_{p_{e_I}}} \tag{1}$$

which can be transformed into equivalent set of first order differential equations composed of energy conservation equation:

$$c_{p_{e_I}}\rho_{e_I}\frac{\partial T_I}{\partial t} = -\frac{\partial q_I}{\partial x} + Q_{v_I} \tag{2a}$$

and Fourier law:

$$q_I = -k_{e_I}\frac{\partial T_I}{\partial x} \tag{2b}$$

Steady capacity of internal heat source Q_{v_I} in source term of Eq. (2a) is defined as follows [39,40]:

$$Q_{v_I} = K_{dys_I}(T_I)E^2 \tag{3}$$

where dissipation coefficient $K_{dys_I}(T_I)$ can be described as a linear regression function [6–8]:

$$K_{dys_I}(T_I) = \pi f \varepsilon_0 \varepsilon''_I(T_I) \approx \mu_{1_I} T_I + \mu_{2_I} \tag{4}$$

Parameters μ_{1_I} and μ_{2_I} in Eq. (4) can be determined experimentally for frozen bed of a material on the basis of calorimetric procedure described in detail elsewhere [10,11].

3.1.2. Dried region

3.1.2.1. Energy conservation. In dried region, additionally, convection is taken into account:

$$\frac{\partial T_{II}}{\partial t} = a_{e_{II}} \frac{\partial^2 T_{II}}{\partial x^2} - \frac{c_{p_g}}{\rho_{bu_{II}} c_{p_{e_{II}}}} \frac{\partial (N_w T_{II})}{\partial x} + \frac{Q_{v_{II}}}{\rho_{bu_{II}} c_{p_{e_{II}}}} \tag{5}$$

which is equivalent to the set of energy conservation equation:

$$c_{p_{e_{II}}} \rho_{bu_{II}} \frac{\partial T_{II}}{\partial t} = -\frac{\partial q_{II}}{\partial x} + \frac{c_{p_w}}{k_{e_{II}}} N_w q_{II} + Q_{v_{II}} \tag{6a}$$

and Fourier law:

$$q_{II} = -k_{e_{II}} \frac{\partial T_{II}}{\partial x} \tag{6b}$$

Steady capacity of internal heat source $Q_{v_{II}}$ is defined analogously as in frozen region:

$$Q_{v_{II}} = K_{dys_{II}}(T_{II}) E^2 \approx \mu_{1_{II}} T_{II} + \mu_{2_{II}} \tag{7}$$

3.1.3. Sublimation front

3.1.3.1. Energy balance. Balance at moving sublimation front is:

$$-k_{e_I} \frac{\partial T_I}{\partial x} + k_{e_{II}} \frac{\partial T_{II}}{\partial x} = N_w \Delta h_s \tag{8}$$

The displacement of the moving boundary is related to the rate of sublimation:

$$N_w = (W_p - W_{eq}) \rho_{bu_{II}} \frac{dX(t)}{dt} \tag{9}$$

3.1.3.2. Temperature of sublimation front T_s. Simultaneous energy and mass balance at the moving boundary gives:

$$\begin{aligned} q_s(t) &= N_w(t) \cdot \Delta H_s = \beta_{II}(t)[C_s(t) - C_L(t)] \Delta h_s \\ &= \beta_{II}(t) \left(\frac{p_s(t)}{T_s(t)} - \frac{p_L}{T_L} \right) \frac{M_w}{R} \Delta h_s \end{aligned} \tag{10}$$

Assuming a thermodynamic equilibrium between water vapor and ice at the moving boundary [3], Eq. (10) can be rearranged into:

$$\frac{\exp\left(\frac{a}{T_s(t)} + b\right)}{T_s(t)} = \frac{q_s(t) R}{\beta_{II}(t) M_w \Delta h_s} + \frac{\exp\left(\frac{a}{T_L} + b\right)}{T_L} \tag{11}$$

where $a = -6320.152$ and $b = 29.558$ [5].

Internal mass transfer coefficient in region *II* can be expressed as:

$$\beta_{II}(t) = \frac{D_{e_{II}}}{L - X(t)} \tag{12}$$

where effective diffusivity $D_{e_{II}}$:

$$\frac{1}{D_{e_{II}}} = \frac{1}{D_K} + \frac{1}{D_M} \tag{13}$$

is a combination of Knudsen diffusivity [49]:

$$D_K = 1.0638 \cdot r_p \sqrt{\frac{R T_{II_{avg}}}{M_w}} \tag{14}$$

and molecular diffusivity [50]:

$$D_M = \frac{1.8829 \cdot T_{II_{avg}}^{3/2} (1/M_w + 1/M_{in})^{1/2}}{P \sigma_{AB}^2 \Omega_{AB}} \tag{15}$$

where σ_{AB} and Ω_{AB} are determined for the system water vapor (A) – air (B) on the basis of tabulated constant of Lennard–Jones forces [50].

Eq. (11) enables estimating of sublimation front temperature T_s at ice front by numerical method e.g. bisection method, in each time step of simulation calculations.

3.1.4. Boundary conditions

At the bottom:

$$-k_{e_I} \left. \frac{\partial T}{\partial x} \right|_{x=0} = 0 \tag{16}$$

and at the exposed surface:

$$k_{e_{II}} \left. \frac{\partial T}{\partial x} \right|_{x=L} = \alpha_{II_\infty} (T_\infty - T_L) \tag{17}$$

$$C_L(t) = C_\infty \tag{18}$$

3.1.5. Initial conditions

For the sake of numerical solution, arbitrary initial position of moving boundary is assumed: $X(t_p) = X_p$. Thus, in frozen layer:

$$T_I(x,\ t_p) = T_s(t_p) \quad \text{for } 0 \leqslant x \leqslant X_p \tag{19}$$

In dried layer initial linear temperature profile is assumed:

$$\frac{T_L(t_p) - T_{II}(x,\ t_p)}{T_L(t_p) - T_s(t_p)} = \frac{L - x(t_p)}{L - X_p} \quad \text{for } X_p \leqslant x \leqslant L \tag{20}$$

3.2. Solution of the mathematical model

3.2.1. Dimensionless variables

Formulated mathematical model of the primary microwave freeze-drying can be rearranged into more convenient form, incorporating following definitions of dimensionless variables:

$$\begin{aligned} &x_I^* = \frac{x_I}{L}, \quad x_{II}^* = \frac{x_{II}}{L}, \quad X^* = \frac{X}{L}, \quad t_I^* = \frac{a_{e_I} t}{L^2}, \quad t_{II}^* = \frac{a_{e_{II}} t}{L^2}, \\ &T_I^* = \frac{T_I - T_{s,3}}{T_{s_{eq}} - T_{s,3}} T_{II}^* = \frac{T_{II} - T_{II_{ref}}}{T_{s_{eq}} - T_{II_{ref}}}, \quad q_I^* = \frac{q_I L}{k_{e_I}(T_{s_{eq}} - T_{s,3})}, \\ &q_{II}^* = \frac{q_{II} L}{k_{e_{II}}(T_{s_{eq}} - T_{II_{ref}})} Q_{v_I}^* = \frac{Q_{v_I} L^2}{k_{e_I}(T_{s_{eq}} - T_{s,3})}, \quad Q_{v_{II}}^* = \frac{Q_{v_{II}} L^2}{k_{e_{II}}(T_{s_{eq}} - T_{II_{ref}})}, \\ &W^* = \frac{W - W_{eq}}{W_p - W_{eq}}, \quad N_w^* = \frac{L c_{pw} N_w}{k_{e_{II}}} \end{aligned} \tag{21}$$

3.2.2. Governing equations in dimensionless form

Equation sets (2) and (6) expressed in terms of the above dimensionless variables are as follows:

$$\frac{\partial T_I^*}{\partial t_I^*} + \frac{\partial q_I^*}{\partial x_I^*} - Q_{v_I}^* = 0 \tag{22a}$$

$$\frac{\partial T_I^*}{\partial x_I^*} + q_I^* = 0 \tag{22b}$$

$$\frac{\partial T_{II}^*}{\partial t_{II}^*} + \frac{\partial q_{II}^*}{\partial x_{II}^*} - Q_{v_{II}}^* - N_w^* q_{II}^* = 0 \tag{23a}$$

$$\frac{\partial T_{II}^*}{\partial x_{II}^*} + q_{II}^* = 0 \quad ?? \tag{23b}$$

3.2.3. Numerical method

Sets (22) and (23) are solved together with adequate initial and boundary conditions by the MacCormack finite-difference method. It is numerical explicit scheme of second order accuracy [51]. Model equations can be rewritten in the following vector form:

$$\frac{\partial E_i}{\partial t_i^*} + \frac{\partial F_i}{\partial x_i^*} + G_i = 0 \quad i = I,\ II \tag{24a}$$

where:

$$E_I = \begin{bmatrix} T_I^* \\ 0 \end{bmatrix} \quad F_I = \begin{bmatrix} q_I^* \\ T_I^* \end{bmatrix} \quad G_I = \begin{bmatrix} -Q_{v_I}^* \\ q_I^* \end{bmatrix} \tag{24b}$$

$$E_{II} = \begin{bmatrix} T_{II}^* \\ 0 \end{bmatrix} \quad F_{II} = \begin{bmatrix} q_{II}^* \\ T_{II}^* \end{bmatrix} \quad G_{II} = \begin{bmatrix} -Q_{v_{II}}^* - N_w^* q_{II}^* \\ q_{II}^* \end{bmatrix} \tag{24c}$$

MacCormack scheme consists of the predictor:

$$\hat{\mathbf{E}}_{i,j}^{n+1} = \mathbf{E}_{i,j}^{n} - \frac{\Delta t_i^*}{\Delta x_i^*}\left(\mathbf{F}_{i,j+1}^{n} - \mathbf{F}_{i,j}^{n}\right) - \Delta t_i^* \cdot \mathbf{G}_{i,j}^{n} \tag{25a}$$

and the corrector:

$$\mathbf{E}_{i,j}^{n+1} = 0.5\left[\mathbf{E}_{i,j}^{n} + \hat{\mathbf{E}}_{i,j}^{n+1} - \frac{\Delta t_i^*}{\Delta x_i^*}\left(\hat{\mathbf{F}}_{i,j}^{n+1} - \hat{\mathbf{F}}_{i,j-1}^{n+1}\right) - \Delta t_i^* \cdot \hat{\mathbf{G}}_{i,j}^{n+1}\right] \tag{25b}$$

where j denotes spatial steps, n – time steps and circumflex – predicted values at time level $n+1$. Detailed equations of MacCormack scheme after incorporating (24b) and (24c) are as follows, for prediction step:

$$\hat{T}_{I,j}^{*n+1} = T_{I,j}^{*n} - \frac{\Delta t_I^*}{\Delta x_I^*}\left(q_{I,j+1}^{*n} - q_{I,j}^{*n}\right) + \Delta t_I^* Q_{v_{I,j}}^* \tag{26a}$$

$$\hat{q}_{I,j}^{*n+1} = \frac{\hat{T}_{I,j}^{*n+1} - \hat{T}_{I,j+1}^{*,n+1}}{\Delta x_I^*} \tag{26b}$$

$$\hat{T}_{II,j}^{*n+1} = T_{II,j}^{*n} - \frac{\Delta t_{II}^*}{\Delta x_{II}^*}\left(q_{II,j+1}^{*n} - q_{II,j}^{*n}\right) + \Delta t_{II}^*\left(Q_{v_{II,j}}^* + N_{w_j}^* q_{II_j}^{*n}\right) \tag{27a}$$

$$\hat{q}_{II,j}^{*n+1} = \frac{\hat{T}_{II,j}^{*n+1} - \hat{T}_{II,j+1}^{*,n+1}}{\Delta x_{II}^*} \tag{27b}$$

and for correction step:

$$T_{I,j}^{*n+1} = 0,5\left[T_{I,j}^{*n} + \hat{T}_{I,j}^{*n+1} - \frac{\Delta t_I^*}{\Delta x_I^*}\left(\hat{q}_{I,j}^{*n+1} - \hat{q}_{I,j-1}^{*n+1}\right) + \Delta t_I^* \hat{Q}_{v_{I,j}}^{*n+1}\right] \tag{28a}$$

$$\hat{q}_{I,j}^{*n+1} = \frac{\hat{T}_{I,j-1}^{*n+1} - \hat{T}_{I,j}^{*n+1}}{\Delta x_I^*} \tag{28b}$$

$$T_{II,j}^{*n+1} = 0,5\left[T_{II,j}^{*n} + \hat{T}_{II,j}^{*n+1} - \frac{\Delta t_{II}^*}{\Delta x_{II}^*}\left(\hat{q}_{II,j}^{*n+1} - \hat{q}_{II,j-1}^{*n+1}\right) - \Delta t_{II}^*\left(\hat{Q}_{v_{II,j}}^* + \hat{N}_{w_j}^* \hat{q}_{II,j}^*\right)\right] \tag{29a}$$

$$\hat{q}_{II,j}^{*n+1} = \frac{\hat{T}_{II,j-1}^{*n+1} - \hat{T}_{II,j}^{*n+1}}{\Delta x_{II}^*} \tag{29b}$$

Dimensionless increment of moving boundary ΔX^*, and dimensionless sample average moisture decrement ΔW^* are derived from Eqs. (8) and (9) in terms of the dimensionless variables (21). They are expressed for region I and region II, respectively:

$$\Delta X_I^{*n+1} = \Delta W_I^{*n+1} = q_{Ij=N}^{*n+1} \cdot Ste_{V_I} \cdot \Delta t_I^*,$$
$$\Delta X_{II}^{*n+1} = \Delta W_{II}^{*n+1} = q_{IIj=N}^{*n+1} \cdot Ste_{V_{II}} \cdot \Delta t_{II}^* \tag{30}$$

where modified Stefan numbers are defined, respectively by:

$$Ste_{v_I} = \frac{\rho_{e_I} c_{p_{e_I}}}{\rho_{bu_{II}}} \frac{(T_{s_{eq}} - T_{s,3})}{\Delta h_s (W_p - W_{eq})}, \quad Ste_{v_{II}} = \frac{c_{p_{eII}} (T_{s_{eq}} - T_{IIref})}{\Delta h_s (W_p - W_{eq})} \tag{31}$$

In each time step the actual values of X^* and W^* are calculated as:

$$X^{*n+1} = X^{*n} + \Delta X_I^{*n+1} + \Delta X_{II}^{*n+1} \tag{32}$$
$$W^{*n+1} = W^{*n} + \Delta W_I^{*n+1} + \Delta W_{II}^{*n+1} \tag{33}$$

Table 1
Physical properties of freeze-dried materials.

Dried material	$d_z \times 10^3$/m	ρ_{e_I}/kg m^{-3}	$\rho_{bu_{II}}$/kg m^{-3}	ε/–	$r_p \times 10^{10}$/m
Silicagel	0.230	1297.4	681	0.67	42.1
Sorbonorit 4	5.268	1048.2	400	0.71	15.2

3.3. Physical properties

For experimental study of the primary freeze-drying at microwave heating two typical adsorbents were chosen: silicagel and Sorbonorit 4 activated carbon. Physical properties of dried material beds are collected in Table 1.

3.4. Numerical results and discussion

Simulations of the primary freeze-drying at microwave heating were performed for $N = 50$ space steps and were stable at given stability condition $\Delta t_i^*/(\Delta x_i^*)^2 \leqslant 1/2$, according to Anderson et al. [52]. Thermophysical parameters which were used in process simulation are as follows for Sorbonorit 4: $a_{e_I} = 1.54 \times 10^{-7}$ m^2/s; $a_{e_{II}} = 3 \times 10^{-9}$ m^2/s; $k_{e_I} = 1.600$ W/(m K); $k_{e_I} = 0.094$ W/(m K); and for Silicagel: $a_{e_I} = 8.97 \times 10^{-7}$ m^2/s; $a_{e_{II}} = 3.13 \times 10^{-8}$ m^2/s; $k_{e_I} = 1.500$ W/(m K); $k_{e_{II}} = 0.039$ W/(m K).

For each experimental run initial position of sublimation front X_p was determined on the basis of measured sample mass decrement during start-up stage of the process. This period from the moment of starting pump until demanded pressure in the vacuum chamber was achieved. It lasted usually 1800s. The same value of X_p was used in numerical calculations.

Exemplary curves of dimensionless moving boundary positions, dimensionless average moisture contents and heat fluxes at moving boundary versus time in microwave freeze-drying of silicagel and Sorbonorit 4 active carbon are shown in Figs. 3 and 4, respectively. In Fig. 3 are presented results for case of constant dissipation coefficients in the frozen and dried material layers of Silicagel. Whereas, in Fig. 4 two runs of theoretical computations assuming both constant and temperature dependant dissipation coefficients in the Sorbonorit 4 layers are shown. Figs. 3 and 4 present also comparison between simulated and experimental results.

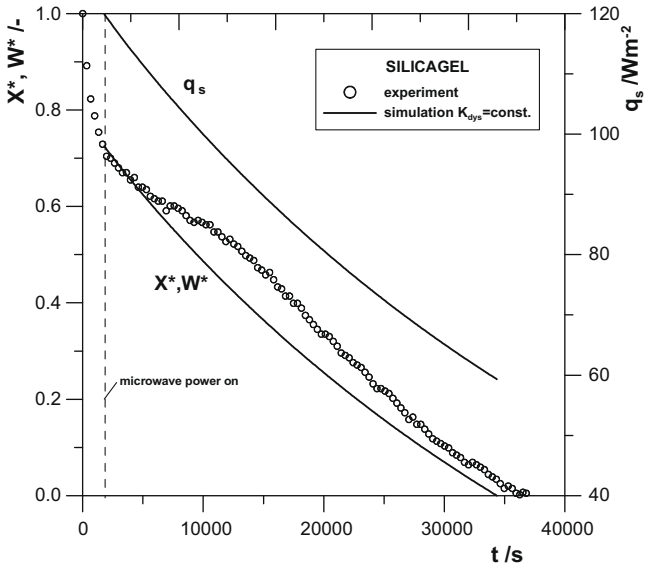

Fig. 3. Dimensionless moving boundary position, dimensionless average moisture content and heat flux at moving boundary versus time in silicagel microwave freeze-drying: $P = 100$ Pa; $L = 0.004$ m; $X_p = 0.0029$ m, $E = 4740$ V/m.

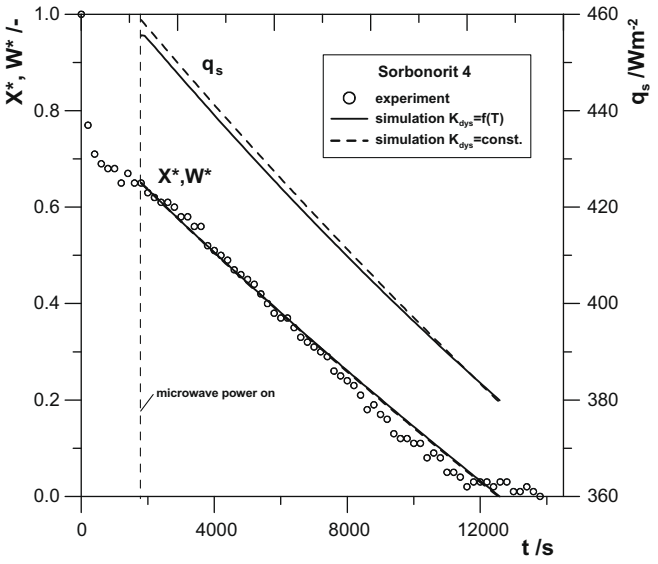

Fig. 4. Dimensionless moving boundary position, dimensionless average moisture content and heat flux at moving boundary versus time in microwave freeze-drying of Sorbonorit 4 active carbon: $P = 100$ Pa; $L = 0.006$ m; $X_p = 0.0039$ m, $E = 460$ V/m.

Calculations for silicagel were performed assuming constant values of dissipation coefficients in the frozen and dried material layers (Fig. 3). Then parameters in the Eqs. (4) and (7), determined on analysis regression basis by fitting model parameters to experimental values, equal: $\mu_{1_I} = \mu_{1_{II}} = 0$ W/(mV^2 K), and $\mu_{2_I} = 0.00159$ W/(mV^2), $\mu_{2_{II}} = 0.00066$ W/(mV^2). In this case μ_{2_I} and $\mu_{2_{II}}$ parameters equal K_{dys_I} and $K_{dys_{II}}$, respectively. Additionally, it is assumed that these values do not depend on the temperature. In this instance, it is realistic assumption because dissipation coefficients measurements for both regions give negligible influence of temperature.

It should be noted that μ_{2_I} and $\mu_{2_{II}}$ parameters (intercepts values in Eqs. (4) and (7)) have similar values, because they were also calculated on the basis of similar effective relative values of adequate loss factors. It was assumed, that the frozen layer consists of ice and silicagel matrix ($\varepsilon''_I = 0.011$), whereas the dried layer consists of vacuum and silicagel matrix ($\varepsilon''_{II} = 0.004$). Effective relative loss factors of the dried and frozen layer according to mixture law were calculated as a nonlinear average of all phase properties, weighted by their volumetric fractions:

$$\varepsilon''_I = \left(\varepsilon\left[\varepsilon''_{ICE}(T)\right]^\kappa + (1-\varepsilon)\left[\varepsilon''_{SOLID}(T)\right]^\kappa\right)^{1/\kappa} \tag{34a}$$

$$\varepsilon''_{II} = \left(\varepsilon\left[\varepsilon''_{VAPOR}(T)\right]^\kappa + (1-\varepsilon)\left[\varepsilon''_{SOLID}(T)\right]^\kappa\right)^{1/\kappa} \tag{34b}$$

where exponent κ is an empirical constant equaled 0.5 [43]. Individual parameters in above equations mean: ε''_{ICE} relative loss factor of the frozen unbounded water in the sample matrix, ε''_{SOLID} relative loss factor of the material solid matrix and ε''_{VAPOR} relative loss factor of the vapor phase frozen unbounded water in the sample matrix.

In order to take into consideration the dependency of dissipation coefficients on material temperature for frozen and dried layers of Sorbonorit 4 active carbon, the following parameters: $\mu_{1_I} = 0.00090$ W/(mV^2 K), $\mu_{2_I} = 0.41148$ W/(mV^2), $\mu_{1_{II}} = 0.00079$ W/(mV^2 K), $\mu_{2_{II}} = 0.30905$ W/(mV^2) were obtained, respectively. They were determined on the basis of measured relationship $Q_{v_i} = K_{dys_i}(T_i)E^2; i = I, II$ according to calorimetric procedure [9,10]. Then liner regression of experimental relation $K_{dys} = f(T)$ was used separately for frozen (I) and dried region (II) to determine μ_{1_i} and $\mu_{2_i}; i = I, II$. Additionally, other calculations were performed assuming constant values of dissipation coefficients in the frozen and dried Sorbonorit 4 layers. In his case averaged parameters in the Eqs. (4) and (7) amount to: $\mu_{2_I} = 0.395$ W/(mV^2) and $\mu_{2_{II}} = 0.299$ W/(mV^2), which correspond to the following calculated effective values of loss factors: $\varepsilon''_I = 2.720$ and $\varepsilon''_{II} = 2.063$, respectively.

For both silicagel (Fig. 3) and Sorbonorit 4 (Fig. 4) calculated heat fluxes at sublimation front decrease during the process, when the thicknesses of the dry layer, having lower dissipation coefficient, increase. As supplied heat flux is the controlling mechanism of freeze-drying process, obtained drying curves have curvature similar to shapes of heat flux at moving boundary versus time $q_s(t)$ relation, which have fairly good agreement with experimental results. For Sorbonorit 4, being lossy dielectric with relatively high

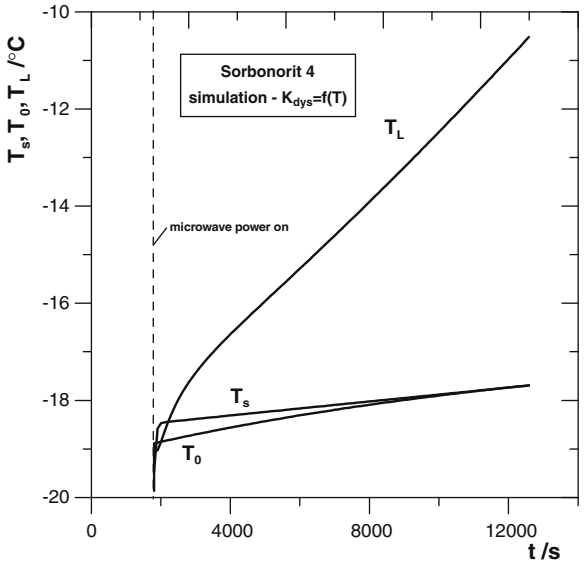

Fig. 5. Simulated temperature of sample surface T_L, sample bottom T_0 and sublimation front T_s in microwave freeze-drying of Sorbonorit 4 active carbon: $P = 100$ Pa; $L = 0.006$ m; $X_p = 0.0039$ m, $E = 460$ V/m.

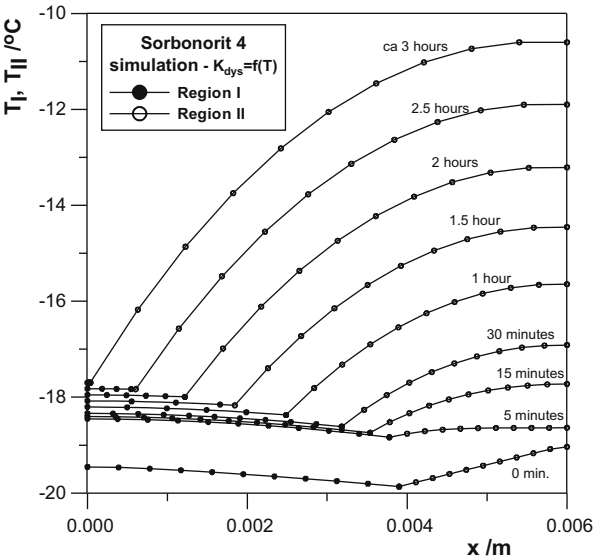

Fig. 6. Simulated temperatures of sample versus position coordinate for various times in microwave freeze-drying of Sorbonorit 4 active carbon: $P = 100$ Pa; $L = 0.006$ m; $X_p = 0.0039$ m, $E = 460$ V/m.

loss factors values for both layers this relation is linear (Fig. 4). Nevertheless, typical microwave freeze-dried biomaterials and foodstuffs have effective loss factor of frozen layer much grater then effective loss factor of dried layer. Therefore their drying curves have common distinct parabolic shape [15,16].

The results of simulations for both variable and constant assuming cases of dissipation coefficients for Sorbonorit 4 activated carbon as well as experimental measurements are compared in Fig. 4. Taking into account temperature dependency of dissipation coefficients, and thereby dielectric loss factors, has no significant influence on simulation results. This results mainly from small material temperature changes during the process observed in Fig. 5 which depicts calculated temperature curves on the surface of dried Sorbonorit 4 sample, at moving boundary and at bottom surface. Furthermore, temperature profiles in both regions for various process times presented in Fig. 6 indicates minimal temperature changes of frozen layer, therefore heat source capacity in this region could be expected constant during the process.

4. Mathematical model of the secondary freeze-drying of random solids at microwave heating

After primary drying, residual moisture content may be as high as 7% [53]. Secondary drying is intended to reduce this to an optimum value for material stability – usually with moisture content between 0.5 and 2.0%.

In secondary stage of the freeze-drying at microwave heating bounded water is removed from the material bed of thickness L showed schematically in Fig. 7.

In formulating of the mathematical model the following assumptions are made:

(i) Average moisture content of material is equal the equilibrium moisture content at average temperature of dried layer at the end of primary freeze-drying $W = W_{eq}$.
(ii) Heat energy is generated volumetrically as a result of microwave absorption and dissipation. Distribution of electric field in a sample is assumed to be uniform.
(iii) There are two mechanisms of mass transport in the material: moisture desorption and diffusion of water vapor throughout the bed.
(vi) Gas phase in dried material and in vacuum chamber consists of water vapor and air (inert).
(v) Adsorption equilibrium is described by multitemperature Langmuir isotherm.

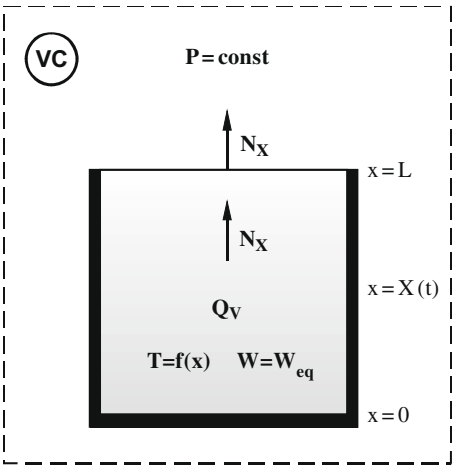

Fig. 7. A physical model of the secondary freeze-drying of random solids at microwave heating.

4.1. Governing equations

4.1.1. Mass conservation

Mass balance of desorbed moisture in gas phase in dried bed is given by:

$$\frac{\partial(y_w \cdot C)}{\partial t} + \frac{\partial(y_w \cdot N_x)}{\partial x} + \frac{\rho_{bu}}{\varepsilon \cdot M_w}\frac{\partial W}{\partial t} = 0 \tag{35}$$

where $y_w + y_{in} = 1$ and $C = P/RT$ is a sum of molar concentrations of components in gas phase including inert (air).

Moisture mass balance in solid phase results from driving force between equilibrium moisture content and actual moisture content of a material:

$$\frac{\partial W}{\partial t} = K(W_r - W) \tag{36}$$

4.1.2. Mass transfer

Kinetic coefficient K in Eq. (36) is calculated applying the linear driving force conception (LDF) [54]:

$$K = \frac{60 \cdot D_{eff}}{d_z^2} \tag{37}$$

The mechanism determining vacuum desorption process is the diffusion rate in material pores which is a combination of Knudsen and surface diffusion. Thus, effective diffusivity can be expressed as:

$$D_{eff} = D_S + D_K \frac{\varepsilon_p M_w}{\rho_p}\frac{\partial y_w^*}{\partial W} \tag{38a}$$

Knudsen diffusivity is defined by [49]:

$$D_K = 1.0638 \cdot r_p \sqrt{\frac{RT}{M_w}} \tag{38b}$$

and surface diffusivity is calculated using Arrhenius type relation [55,56]:

$$D_S = D_{S0} \exp\left(-\frac{E_0}{RT}\right) \tag{38c}$$

Adsorption equilibrium is expressed by multitemperature extended Langmuir isotherm [57]:

$$W_r = W_0 \exp\left(\frac{a}{T}\right)\left[\frac{b \cdot \exp\left(\frac{c}{T}\right)P \cdot y_w}{1 + b \cdot \exp\left(\frac{c}{T}\right)P \cdot y_w}\right] \tag{39}$$

Thus, the derivative $\frac{\partial y_w^*}{\partial W}$ in Eq. (38a) can be solved analytically as:

$$\frac{\partial y_w^*}{\partial W} = \frac{W_0 \exp\left(\frac{a}{T}\right)}{b \exp\left(\frac{c}{T}\right)P\left[W - W_0 \exp\left(\frac{a}{T}\right)\right]^2} \tag{40}$$

4.1.3. Heat transfer

Quasi-homogeneous heat balance equation can be expressed as:

$$-k_e \frac{\partial^2 T}{\partial x^2} + N_x \sum_{i=1}^{s} y_i c_{pg_i}\frac{\partial T}{\partial x} + c_\Sigma \frac{\partial T}{\partial t} + \Delta H_{ads}\frac{\rho_{bu}}{M_w}\frac{\partial W}{\partial t} - Q_v = 0 \tag{41}$$

where c_Σ denotes total volumetric specific heat:

$$c_\Sigma = \rho_{bu}(c_s + W c_a) + \varepsilon \cdot C \sum_{i=1}^{s} y_i c_{pg_i} \tag{42}$$

Isosteric adsorption heat of water vapor in dried material included in Eq. (41) is estimated from Clausius–Clapeyron type equation [58,59]:

$$\Delta H_{ads} = -RT^2\left(\frac{\partial \ln P}{\partial T}\right)_W \tag{43}$$

Above equation after incorporating multitemperature Langmuir isotherm can be rewritten in analytical form:

$$\Delta H_{ads} = -\frac{R \cdot W_o \exp(a/T)}{W_o \exp(a/T) - W}\left(a + c - \frac{W \cdot c}{W_o \exp(a/T)}\right) \tag{44}$$

Source term in Eq. (41) resulting from dissipation of microwave energy in material volume is defined as:

$$Q_v = K_{dys} E^2 \tag{45}$$

Dissipation coefficient K_{dys} in Eq. (45) is expressed as a linear function of material temperature:

$$K_{dys}(T) \approx \mu_1 T + \mu_2 \tag{46}$$

where parameters μ_1 and μ_2 are determined by linear regression of experimental data [11].

4.1.4. Momentum balance

Pressure drop along the sample axis is described by Ergun relation [60]:

$$\frac{\partial P}{\partial x} = -\frac{\eta}{C \cdot k_D} N_x - \sum_{i=1}^{s} y_i M_i \frac{k_E}{C k_D} N_x^2 \tag{47}$$

Parameter k_D in above Equation defines permeability of dried bed and parameter k_E describes inertial effect:

$$k_D = \frac{d_z^2 \varepsilon^3}{150(1-\varepsilon)^2}; k_E = \frac{1.75 d_z}{150(1-\varepsilon)} \tag{48}$$

where d_z is the equivalent diameter of adsorbent grain and ε denotes bed porosity.

In order to simplify calculation a following relation defining molar flux density of water vapor is derived [61]:

$$N_x = -\frac{2Ck_D\eta^{-1}\partial P/\partial x}{1 + \sqrt{1 + 4C \cdot \left(\sum_{i-1}^{s} y_i M_i\right) k_D k_E \eta^{-2} |\partial P/\partial x|}} \tag{49}$$

4.1.5. Boundary and initial conditions

Formulated mathematical model is solved together with the following boundary and initial conditions:

$$\frac{\partial y_i}{\partial x} = 0; \quad \frac{\partial P}{\partial x} = 0; \quad \frac{\partial T}{\partial x} = 0 \quad \text{for } x = 0 \tag{50a}$$

$$\frac{\partial T}{\partial x} = 0; \quad P = P(t) \quad \text{for } x = L \tag{50b}$$

$$W = W(x,0); \quad T = T(x,0); \quad P = P(x,0) \quad \text{for } t = 0 \tag{50c}$$

4.2. Solution of the mathematical model

4.2.1. Dimensionless variables

Model equations can be expressed in more convenient dimensionless form incorporating the following definitions of dimensionless variables:

$$t^* = \frac{a_e t}{L^2}; \quad x^* = \frac{x}{L}; \quad \omega = \frac{P}{\Delta P}; \quad T^* = \frac{T - T_p}{\Delta T} \tag{51a}$$

$$W^* = \frac{W - W_r}{W_p - W_r}; \quad C_w^* = \frac{y_w C}{C_{w0}}; \quad Q_v^* = Q_v L^2/(k_e \Delta T) \tag{51b}$$

where pressure and temperature are normalized relatively to arbitrary chosen increments ΔP and ΔT respectively.

4.2.2. Governing equations in dimensionless form

Mathematical model after transformation consists of mass balance in gas phase:

$$a_e C_{w0} \frac{\partial C_w^*}{\partial t^*} + L \frac{\partial (y_w \cdot N_x)}{\partial x^*} + \frac{a_e \rho_{bu}(W_p - W_r)}{\varepsilon M_w} \frac{\partial W^*}{\partial t^*} = 0 \tag{52}$$

mass balance in solid phase:

$$\frac{\partial W^*}{\partial t^*} = -\frac{L^2}{a_e} K W^* \tag{53}$$

quasi-homogeneous heat balance:

$$-k_e \frac{\partial^2 T^*}{\partial x^{*2}} + L N_x \sum_{i=1}^{s} y_i c_{pg_i} \frac{\partial T^*}{\partial x^*} + L c_\Sigma \frac{\partial T^*}{\partial t^*} + \frac{a_e (W_p - W_r)\rho_{bu}}{\Delta T} \frac{\Delta H_{ads}}{M_w} \frac{\partial W^*}{\partial t^*} - k_e Q_v^* = 0 \tag{54}$$

and Ergun equation:

$$\Delta P \frac{\partial(\omega)}{\partial x^*} = -\frac{L\eta}{C k_D} N_x - \left(\sum_{i=1}^{s} y_i M_i\right) \frac{L k_E}{C k_D} N_x^2 \tag{55}$$

where W^* is expressed by multitemperature extended Langmuir isotherm (39).

4.2.3. Numerical method

Mathematical model is solved numerically by means of lines method which requires transformation of partial differential equations into set of ordinary differential equations for time derivatives, and approximation of space derivatives by adequate finite differences [62].

Fixed-bed region is divided into $N-1$ parts with N nodal points as is shown in Fig. 8, and value j denotes space steps.

Applying central finite-difference scheme for second order approximation of first and second order derivatives for $j = 1, \ldots, N-1$, the water vapor mass balance becomes:

$$\frac{d(C_w^*)_j}{dt^*} = -\frac{L}{a_e C_{w0}} \frac{(y_w \cdot N_x)_{j+1} - (y_w \cdot N_x)_{j-1}}{2\Delta x^*} - \frac{\rho_{bu}(W_p - W_r)_j}{C_{w0} \varepsilon M_w} \frac{d(W^*)_j}{dt^*} \tag{56}$$

The mass balance in the dried material:

$$\frac{(dW^*)_j}{dt^*} = -\frac{L^2}{a_e} K (W^*)_j \quad \text{for } j = 1, \ldots, N-1 \tag{57}$$

The heat balance equation:

$$\frac{dT_j^*}{dt^*} = \frac{k_e}{L c_\Sigma} \frac{T_{j+1}^* - 2T_j^* + T_{j-1}^*}{\Delta x^{*2}} - \frac{N_x}{c_\Sigma} \sum_{i=1}^{s} y_i c_{pg_i} \frac{T_{j+1}^* - T_{j-1}^*}{2\Delta x^*} + -\frac{a_e \rho_{bu}(W_p - W_r)}{L c_\Sigma \Delta T} \frac{\Delta H_{ads}}{M_w} \frac{d(W^*)_j}{dt^*} + \frac{k_e}{L c_\Sigma} Q_{v_j}^* \quad \text{for } j = 1, \ldots, N-1 \tag{58}$$

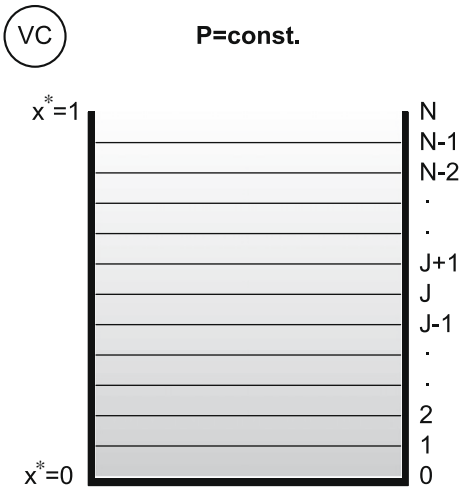

Fig. 8. Division of dried material layer into N sections in numerical method of lines.

The pressure drop in dried material:

$$\frac{\omega_{j+1}-\omega_{j-1}}{2\Delta x^*} = -\frac{L\eta}{\Delta P C k_D} N_x - \left(\sum_{i=1}^{s} y_i M_i\right)\frac{Lk_E}{\Delta P C k_D} N_x^2 \quad \text{for } j = 1,\ldots,N-1 \tag{59}$$

For $j = N$ dimensionless pressure drop is equal to dimensionless pressure in the vacuum chamber $\omega_{VC} = (P_{VC} - P_0)/\Delta P = \text{const}$. For $j = 0$ differential $\left.\frac{\partial \omega_j}{\partial x^*}\right|_{j=0}$ is replaced by a forward difference:

$$\frac{\partial \omega_j}{\partial x^*} = \frac{-3\omega_j + 4\omega_{j+1} - \omega_{j+2}}{2\Delta x^*} = 0 \quad \text{for } j = 0 \tag{60}$$

which can be solved for ω_0 to yield $\omega_0 = (4\omega_1 - \omega_2)/3$. Molar flux of water vapor:

$$N_x = -\frac{2Ck_D\eta^{-1}\left[(\omega_{j+1}-\omega_{j-1})/2\Delta x^*\right]}{1+\sqrt{1+4C\left(\sum_{i-1}^{s} y_i M_i\right)k_D k_E \eta^{-2}\left|\left[(\omega_{j+1}-\omega_{j-1})/2\Delta x^*\right]\right|}} \tag{61}$$

Temperature and concentration at nodes 0 and N were computed according to suitable boundary conditions defined by Eq. (50a–c).

As a result of computations temperature and water concentration distributions in dried material can be calculated.

4.3. Physical properties

In theoretical analysis the vacuum desorption of water in Zeolite DAY-20F is considered. Parameters of multitemperature Langmuir isotherm for water–Zeolite DAY-20F system listed in Table 2 [1,4] were approximated by nonlinear Levenberg–Marquardt estimation of data within temperature range of 293—373 K [61]. Multitemperature Langmuir isotherm of water vapor on Zeolite DAY-20F in wide range of pressure is shown in Fig. 9. Additionally multitemperature Langmuir isostere for the same system is depicted in Fig. 10. Physical properties of Zeolite DAY-20F assumed at average bed temperature 303.15 K and process pressure 100 Pa are as follows: $k_e = 0.025\ \text{W/(m K)}, c_s = 900\ J/(\text{kg K}), \rho_b = 500\ \text{kg/m}^3; \varepsilon = 0.677$.

Table 2
Constants of multitemperature Langmuir isotherm equation for water–Zeolite DAY-20F system.

Component	Constants of multitemperature Langmuir isotherm equation			
	W_0/kg kg^{-1}	a/K	b/Pa^{-1}	c/K
Water	0.370300	1387.82	0.170×10^{-6}	1511.02

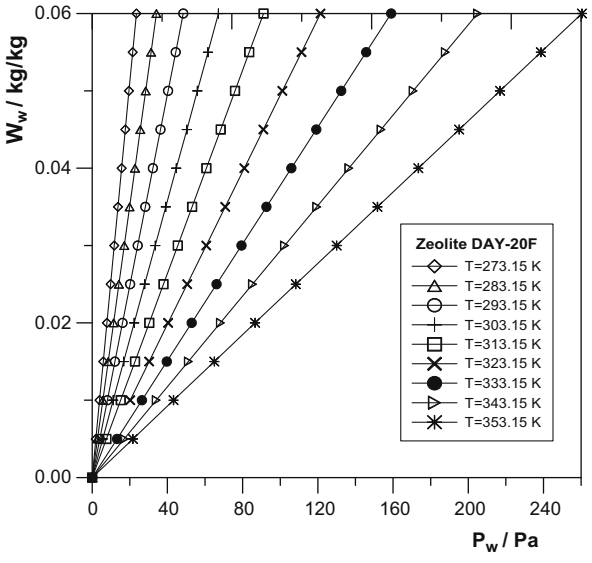

Fig. 9. Multitemperature adsorption isotherm of water vapor on Zeolite DAY-20F.

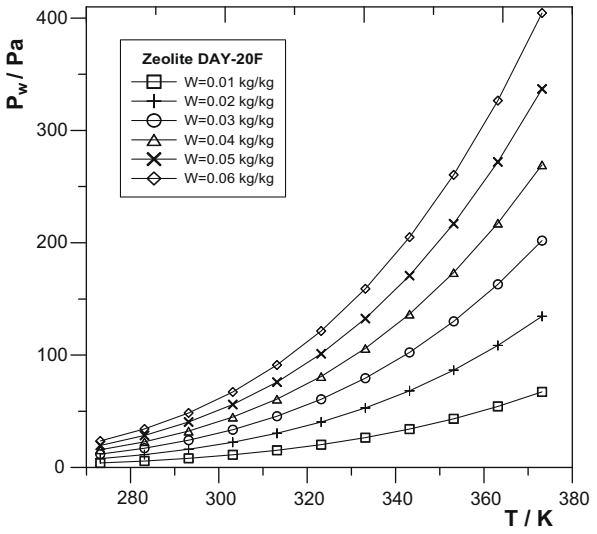

Fig. 10. Multitemperature adsorption isosteres of water vapor on Zeolite DAY-20F.

5. Results and discussion

During the primary freeze-drying stage equilibrium water vapor pressure in region *II* equals approximately vapor pressure at sublimation front, i.e. 100 Pa. Equilibrium material (Zeolite DAY-20F) moisture content relative to that pressure equals about 0.05 kg/kg for maximal material temperature: 323 K (Fig. 9). Thus for dried layer temperatures range (region *II*), taking place during primary freeze-drying (below 323 K) moisture desorption does not exist.

Formulated here mathematical model of the secondary vacuum freeze-drying at microwave heating consisting of Eqs. (55)–(59)

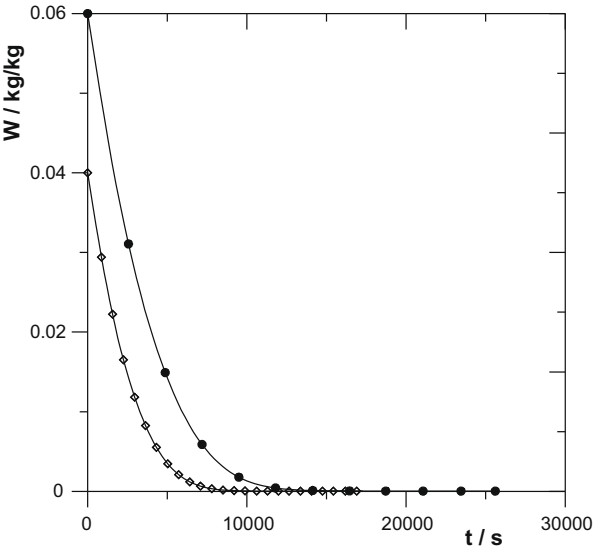

Fig. 11. Moisture content of Zeolite DAY-20F versus time: $P = 100$ Pa; $L = 0.04$ m; $W_p = 0.04$ and 0.06 kg/kg; $E = 2500$ V/m; $Q_v = 6588\ W/m^3$; $\mu_1 = 1.107 \times 10^{-6}$ W/(mV^2 K); $\mu_2 = 1.021 \times 10^{-3}$ W/(mV^2).

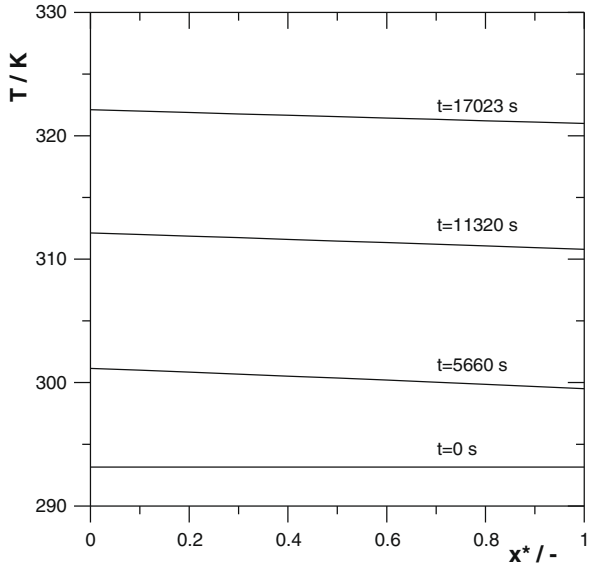

Fig. 12. Temperature profiles of Zeolite DAY-20F for various process times: $P = 100$ Pa; $L = 0.04$ m; $W_p = 0.04$ kg/kg; $E = 2500$ V/m; $Q_v = 6588$ W/m^3; $\mu_1 = 1.107 \times 10^{-6}$ W/(mV^2 K); $\mu_2 = 1.021 \times 10^{-3}$ W/(mV^2).

with adequate initial and boundary conditions (50) was solved by 4thorder Runge–Kutta method with the following process parameters: $L = 0.004$ or 0.006 m, $W_p = 0.04$ or 0.06 kg/kg, $\mu_1 = 1.107 \times 10^{-6}$ W/(mV^2 K), $\mu_2 = 1.021 \times 10^{-3}$W/(mV^2), $E = 2500$ V/m and initial bed temperature $T(x,0) = 293.15$ K. Calculated dissipation coefficient at this conditions amounts to $K_{dys} = 1.054 \times 10^{-3}$ and average capacity of internal volumetric heat source throughout the material equals: $Q_v = 6588$ W/m^3. Obtained results of numerical simulation are presented in Figs. 11 and 12.

Moisture contents versus time for two initial bed moisture contents $W_p = 0.04$ and 0.06 kg/kg in Zeolite DAY-20F bed of thickness $L = 0.04$ m are shown in Fig. 11.

Fig. 12 depicts dried bed temperatures versus dimensionless positions in the material layer, for various process times at sample thickness $L = 0.04$ m and initial moisture content $W_p = 0.04$ kg/kg.

6. Conclusions

The mathematical model of both primary and secondary freeze-drying stages of random solids at microwave heating was developed. Experimental and theoretical investigations of the primary freeze-drying at microwave heating were presented for two selected materials: Sorbonorit 4 activated carbon and Silicagel beds. Furthermore, theoretical analysis of the secondary freeze-drying at microwave heating was performed for Zeolite DAY-20F bed.

For dried materials such as used here, characterized by considerable internal porosity, primary freeze-drying stage is not sufficient to remove entire moisture contained in the dried bed. During primary freeze-drying at microwave heating free, interstitial moisture is removed. Secondary freeze-drying stage is then necessary to remove residual moisture which may be as high as 7%, after primary stage.

Kinetics of the microwave freeze-drying process is enhanced in comparison with freeze-drying at conventional heating. It is caused mainly by the fact, that in conventional heating temperature and mass transfer gradients in the dried material have opposite directions. On the contrary, in freeze-drying process at microwave heating both temperature, and mass transfer gradients are cocurrent. It is very convenient phenomenon from point of view of the qualitative final dried material properties.

Assumption of constant electric field strength in a dried material is valid for dimensions samples up to half wavelength order in mono-modal resonant cavities. Formulated mathematical model can be also applicable in microwave heating of samples dimensions equaled multiple wavelengths in multimodal applicators with uniform distribution of electric field strength.

The model for secondary freeze-drying at microwave heating takes into account mass transfer resistances which arise in vacuum desorption. The LDF mass transfer model with a variable, lumped-resistance coefficient K was used. This numerical model was applied to perform computer simulation of the vacuum desorption of pure water from zeolite DAY-20F.

The recorded current signal of the microwave detector coupled with the magnetic loop in the bottom wall of the microwave applicator used in investigations was not constant during an experimental run. It may indicate that electric field strength in a dried sample varies during the process. These changes were not significant, however taking them into account in mathematical modeling would require: derivation of complex dependency between electric field strength and sublimation front position as well as the temperature distributions in sample layers. Such studies should be taken into account in the future modeling developments.

In theoretical investigations of both the primary and secondary process stages, source terms in model equations were calculated at electromagnetic wave frequency of 2.45 GHz as a function of averaged electric field strength and material dielectric properties. Dependency of dissipation coefficient on temperature is taken into account and simplified by linear regression function with parameters μ_1 and μ_2. Nevertheless, for some dried materials dissipation coefficient can be assumed constant and then parameter $\mu_1 = 0$ and μ_2 is equaled K_{dys}.

Experimental verification of the model simulations of the primary freeze-drying at microwave heating approved its fairly good usefulness for design applications. Furthermore, mathematical model of the vacuum desorption in the secondary freeze-drying enables predictions of the drying kinetics for the random solids.

Acknowledgement

This work was supported by Grant No. 3 T09C 022 27 from the Polish State Committee for Scientific Research.

References

[1] J. Nastaj, B. Ambrożek, Modeling of vacuum desorption of multicomponent moisture in freeze drying, Trans. Porous Media 66 (2007) 201–218.
[2] J.H. Nam, C.S. Song, Numerical simulation of conjugate heat and mass transfer during multi-dimensional freeze drying of slab-shaped food products, Int. J. Heat Mass Transfer 50 (23–24) (2007) 4891–4900.
[3] J. Nastaj, A parabolic cylindrical Stefan problem in vacuum freeze drying of random solids, Int. Commun. Heat Mass Transfer 30 (1) (2003) 93–104.
[4] J. Nastaj, B. Ambrożek, Modeling of vacuum desorption in freeze-drying process, Drying Technol. 23 (8) (2005) 1693–1709.
[5] W.W. Rothmayr, Basic knowledge of freeze drying, in: S.A. Goldblith, L. Rey, W.W. Rothmayr (Eds.), Freeze-drying and Advanced Food Technology, Academic Press, London, 1975 (Chapter 15).
[6] Y.C. Fey, M.A. Boles, Analytical study of vacuum-sublimation in an initially partially filled frozen porous medium with recondensation, Int. J. Heat Mass Transfer 31 (1988) 1645–1653.
[7] A.I. Liapis, H. Sadikoglu, Mathematical modelling of the primary and secondary drying stages of bulk solution freeze-drying in trays: parameter estimation and model discrimination by comparison of theoretical results with experimental data, Drying Technol. 15 (3,4) (1997) 791–810.
[8] A.I. Liapis, R. Bruttini, H. Sadikoglu, Optimal control of the primary and secondary drying stages of the freeze drying of pharmaceuticals in vials, in: Proceedings of the 12th IDS, 2000, pp. 115–124.
[9] J. Nastaj, K. Witkiewicz, Experimental and simulation studies of primary vacuum freeze-drying process of random solids at microwave heating, Int. Commun. Heat Mass Transfer 35 (2008) 430–438.

[10] J. Nastaj, K. Witkiewicz, Experimental identification of internal heat source capacity in vacuum freeze drying of random solids at microwave heating, Chem. Process Eng. (Inżynieria Chemiczna i Procesowa) 28 (4) (2007) 1033–1044.
[11] K. Witkiewicz, Modelowanie numeryczne suszenia sublimacyjnego materiałów ziarnistych przy ogrzewaniu mikrofalowym (The numerical modeling of freeze-drying of granular solids at microwave heating), Ph.D. Dissertation, Szczecin University of Technology, Szczecin, 2006 (in Polish).
[12] Z. Tao, H. Wu, G. Chen, H. Deng, Numerical simulation of conjugate heat and mass transfer process within cylindrical porous media with cylindrical dielectric cores in microwave freeze-drying, Int. J. Heat Mass Transfer 48 (2005) 561–572.
[13] W. Wang, G. Chen, Heat and mass transfer model of dielectric-material-assisted microwave freeze-drying of skim milk with hygroscopic effect, Chem. Eng. Sci. 60 (2005) 6542–6550.
[14] T.K. Ang, J.D. Ford, D.C.T. Pei, Microwave freeze-drying of food: a theoretical investigation, Int. J. Heat Mass Transfer 20 (1977) 517–526.
[15] Y.H. Ma, P.R. Peltre, Freeze dehydration by microwave energy: Part I. Theoretical investigation, AIChE J. 21 (2) (1975) 335–344.
[16] Y.H. Ma, P.R. Peltre, Freeze dehydration by microwave energy: Part II. Experimental study, AIChE J. 21 (2) (1975) 344–350.
[17] A.I. Liapis, R. Bruttini, A mathematical model for the spray freeze drying process: the drying of frozen particles in trays and in vials on trays, Int. J. Heat Mass Transfer 52 (2009) 100–111.
[18] A.K. Hagi, N. Amanifard, Analysis of heat and mass transfer during microwave drying of food products, Braz. J. Chem. Eng. 25 (3) (2008) 491–501.
[19] S.J. Kowalski, Modeling of capillary-porous materials microwave drying (in Polish), Chem. Process Eng. (Inżynieria Chemiczna i Procesowa) 25 (3/2) (2004) 1139–1143.
[20] P. Ratanadecho, K. Aoki, M. Akahori, Experimental and numerical study of microwave drying in unsaturated porous material, Int. Commun. Heat Mass Transfer 28 (5) (2001) 605–616.
[21] I.W. Turner, J.R. Puiggali, W. Jomaa, A numerical investigation of combined microwave and convective drying of a hygroscopic porous material: a study based on pine wood, Chem. Eng. Res. Des. 76 (2) (1998) 193–209.
[22] W. Kaensup, S. Wongwises, Drying of pepper seeds using a combined microwave/fluidized bed, Drying Technol. 16 (3–5) (1998) 853–862.
[23] L.E. Campana, M.E. Sempe, Physical, chemical and baking properties of wheat dried with microwave energy, Cereal Chem. 70 (6) (1993) 760–762.
[24] E.U. Schlunder, Microwave drying of ceramic spheres and cylinders, Chem. Eng. Res. Des. 71 (6) (1993) 622–628.
[25] R.M. Perkin, The drying of porous materials with electromagnetic energy generated at radio and microwave frequencies, in: R.J. Wakeman (Ed.), Progress in Filtration and Separation, vol. 3, Elsevier, Amsterdam, 1983, pp. 205–266.
[26] I.W. Truner, P.G. Jolly, Combined microwave and convective drying a porous material, Drying Technol. 9 (5) (1991) 1209–1269.
[27] I.W. Truner, P.G. Jolly, The effect of dielectric properties on microwave drying kinetics, J. Microw. Power 25 (4) (1990) 211–223.
[28] J.L. Grolmes, T.L. Bergman, Dielectrically – assisted drying of non-hygroscopic porous material, Drying Technol. 8 (5) (1990) 953–975.
[29] S.K. Samanta, T. Basak, B. Sengupta, Theoretical analysis on microwave heating of oil–water emulsions supported on ceramic, metallic or composite plater, Int. J. Heat Mass Transfer 51 (2008) 6136–6156.
[30] T. Basak, K. Aparna, A. Meenakshi, A.R. Balakrishnan, Effect of ceramic supports on microwave processing of porous food samples, Int. J. Heat Mass Transfer 49 (2006) 4325–4339.
[31] H. Zhang, A.K. Datta, I.A. Taub, Electromagnetics, heat transfer and thermokinetics in microwave sterilization, AIChE J. 47 (9) (2001) 1957–1968.
[32] P. Ratanadecho, K. Aoki, M. Akahori, A numerical and experimental investigation of the modelling of microwave melting of frozen packed beds using a rectangular ave guide, Int. Comm. Heat Mass Transfer 28 (6) (2001) 751–762.
[33] M.E.C. Oliveira, A.S. Franca, Finite element analysis of microwave heating of solid products, Int. Comm. Heat Mass Transfer 27 (4) (2000) 527–536.
[34] E.T. Thostenson, T.W. Chou, Microwave processing: fundamentals and applications, Composites A 30 (1999) 1055–1071.
[35] H.H.J. Remmen, C.T. Ponne, H.H. Nijhuis, P.V. Bartels, P.J.A.M. Kerkhof, Microwave heating distributions in slabs, spheres and cylinders with relation to food processing, J. Food Sci. 61 (6) (1996) 1105–1113.
[36] F. Liu, I. Turner, M. Bialkowski, A finite difference time-domain simulation of power density distribution in a dielectric loaded microwave cavity, J. Microw. Power 29 (3) (1994) 138–147.
[37] A. Datta, Heat and mass transfer in the microwave processing of food, Chem. Eng. Prog. (1990) 47–53.
[38] R.V. Decareau, R.A. Peterson, Microwave Processing and Engineering, Ellis Horwood Ltd., Chishester, England, 1986.
[39] R. Meredith, Engineers' Handbook of Industrial Microwave Heating, IEE, London, 1998.
[40] A.C. Metaxas, Foundations of Electroheat: A Unified Approach, John Wiley & Sons, New York, 1996.
[41] J.E. Atwater, R.R. Wheeler Jr., Microwave permittivity and dielectric relaxation of a high surface area activated carbon, Appl. Phys. A 79 (2004) 125–129.
[42] Y.-C. Chen, P.-S. Cheng, C.-F. Yang, W.-C. Tzou, Substitution of CaO by BaO to improve the microwave dielectric properties of $CaO–Li_2O–Sm_2O_3–TiO_2$, Ceram. Int. 27 (7) (2001) 809–813.
[43] C. Péré, E. Rodier, O. Louisnard, Microwave vacuum drying of porous media: verification of a semi-empirical formulation of the total absorbed power, Drying Technol. 19 (6) (2001) 1005–1022.
[44] N.N. Grinchik, P.V. Akulich, A.L. Adamovich, P.S. Kuts, S.P. Kundas, Modeling of nonisothermal heat and moisture transfer in capillary-porous media in periodic microwave heating, J. Eng. Phys. Thermophy. 80 (1) (2007) 1–10.
[45] N.V. Men'shutina, M.G. Gordienko, A.A. Voinovskii, T. Kudra, Dynamic criteria for evaluating the energy consumption efficiency of drying equipment, Theor. Found. Chem. Eng. 39 (2) (2005) 158–162.
[46] A. Brykov, L. Rikenglaz, Simplified theory of microwave drying of alkali metal silicate solutions with arbitrary values of SiO2/M2O mole ratio, J. Microw. Power Electromagn. Energy 35 (3) (2000) 191–196.
[47] A.A. Krupa, M.E. Il'chenko, V.A. Mikhailenko, V.A. Makogon, Microwave technology for drying ceramic materials, Glass Ceram. 50 (1) (1993) 34–38.
[48] W. Kamiński, Hyperbolic heat conduction equation for materials with a nonhomogeneous inner structure, ASME J. Heat Transfer 112 (1990) 555–560.
[49] J.M. Coulson, J.F. Richardson, R.K. Sinnott, Chemical Engineering, vol. 6, Butterworth Heinemann, Oxford, 1999.
[50] B.E. Poling, J.M. Prausnitz, J.P. O'Connell, The Properties of Gases and Liquids, fifth ed., McGraw-Hill, New York, 2001.
[51] L. Malinowski, Effect of relaxation of internal heat source capacity in the temperature field in the semi-infinite body, Int. Commun. Heat Mass Transfer 18 (4) (1991) 523–530.
[52] D.A. Anderson, J.C. Tannehil, R.H. Pletcher, Comput. Fluid Mech. Heat Transfer, McGraw-Hill, New York, 1984.
[53] T.W. Rowe, J.W. Snowman, Edwards Freeze-drying Handbook, Crawley, Cambridge, 1978.
[54] E. Glueckauf, Theory of chromatography, Trans. Faraday Soc. 51 (1955) 1540–1551.
[55] J.-H. Yun, D.-K. Choi, S.-H. Kim, Equilibria and dynamics for mixed vapors of BTX in an activated carbon bed, AIChE J. 45 (4) (1999) 751–760.
[56] J.-H. Yun, D.-K. Choi, H. Moon, Benzene adsorption and hot purge regeneration in activated carbon needs, Chem. Eng. Sci. 55 (23) (2000) 5857–5872.
[57] M.H. Chahbani, V. Tondeur, Pressure drop in fixed-bed adsorbers, Chem. Eng. J. 81 (2001) 23–34.
[58] T.L. Hill, Statistical mechanics of adsorption. V. Thermodynamics and heat of adsorption, J. Chem. Phys. 17 (1949) 520–535.
[59] D.D. Do, Adsorption Analysis: Equilibria and Kinetics, Imperial College Press., London, 1998.
[60] S. Ergun, Fluid flow through packed column, Chem. Eng. Prog. 48 (1952) 89–94.
[61] L.M. Sun, N. Ben Amar, F. Meunier, Numerical study on coupled heat and mass transfer in an adsorber with external fluid heating, Heat Recovery Syst. CHP 15 (1995) 19–29.
[62] W.E. Schiesser, The Numerical Method of Lines: Integration of Partial Differential Equations, Academic Press, New York, 1991.